

Functionally Relevant Coupled Dynamic Profile of Bacteriorhodopsin and Lipids in Purple Membranes<sup>†</sup>Miya Kamihira<sup>‡</sup> and Anthony Watts\*

Biomembrane Structure Unit, Department of Biochemistry, Oxford University, South Parks Road, Oxford OX1 3QU, U.K.

Received August 31, 2005; Revised Manuscript Received January 27, 2006

**ABSTRACT:** The dynamics of bacteriorhodopsin (bR) and the lipid headgroups in oriented purple membranes (PMs) was determined at various temperatures and relative humidity (rh) using solid-state NMR spectroscopy. The <sup>31</sup>P NMR spectra of the  $\alpha$ - and  $\gamma$ -phosphate groups in methyl phosphatidylglycerophosphate (PGP-Me), which is the major phospholipid in the PM, changed sensitively with hydration levels. Between 253 and 233 K, the signals from a fully hydrated sample became broadened similarly to those of a dry sample at 293 K. The <sup>15</sup>N cross polarization (CP) NMR spectral intensities from [<sup>15</sup>N]Gly bR incorporated into fully hydrated PMs were suppressed in <sup>15</sup>N CP NMR spectra at 293 K compared with those of dry membranes but gradually recovered at low temperatures or at lower hydration (75%) levels. The suppression of the NMR signals, which is due to interference with proton decoupling frequency (~45 kHz), coupled with short spin–spin relaxation times ( $T_2$ ) indicates that the loops of bR, in particular, have motional components around this frequency. The motion of the transmembrane  $\alpha$ -helices in bR was largely affected by the freezing of excess water at low temperatures. While between 253 and 233 K, where a dynamic phase transition-like change was observed in the <sup>31</sup>P NMR spectra for the phosphate lipid headgroups, the molecular motion of the loops and the C- and N-termini slowed, suggesting lipid–loop interactions, although protein–protein interactions between stacks cannot be excluded. The results of  $T_2$  measurements of dry samples, which do not have proton pumping activity, were similar to those for fully hydrated samples below 213 K where the M-intermediates can be trapped. These results suggest that motions in the 10s  $\mu$ s correlation regime may be functionally important for the photocycle of bR, and protein–lipid interactions are motionally coupled in this dynamic regime.

Bacteriorhodopsin (bR)<sup>1</sup> is one of the most extensively studied light-driven proton pumps in *Haloarchaea*. It contains seven transmembrane  $\alpha$ -helices surrounding the retinal chromophore and has been the structural paradigm of G-protein-coupled receptors and other membrane proteins (1–5). It forms a protein–lipid complex of defined composition in the purple membrane (PM), where bR is arranged in trimeric units assembled in 2D crystalline patches in a hexagonal lattice. High-resolution X-ray (6–11) and electron (12, 13) crystallography have been used to determine the 3D structure of bR and the structural changes at K, L, M, N, and O photointermediates to understand the unidirectional

translocation of proton pumping activity (14–23). Solid-state NMR spectroscopy has been used to provide detailed information about the local structural changes of retinal (24, 25) around the key residues involved in proton pumping activity (26, 27) and the local mobility of bR (28–30) under physiological conditions. Also, the structure and orientation of some  $\alpha$ -helices of membrane-embedded bR have been determined by polarization inversion spin exchange at the magic angle (PISEMA), <sup>1</sup>H-<sup>15</sup>N heteronuclear correlation spectroscopy (HETCOR) (31), and magic angle oriented sample spinning (MAOSS) (32) NMR methods, and it was demonstrated that the extracellular half of helix B is tilted at less than 5° from the membrane normal and that the tilt angle of the cytoplasmic side of helix A is 18–22° (31).

Although *structural* studies have provided a remarkably detailed view of the protein, including details of the organization of key residues and water molecules to give a quantitative understanding of its proton pumping activity, other regions such as the loops and headgroups of phospholipids in the PM are less studied because of high mobility and concomitant poor ordering, making them less amenable to methods requiring rigid atom positions.

Protein dynamics is intimately connected with activity and function. In particular, mobile regions such as loops can play a key role in signal transaction or ligand binding, such as in G-coupled receptors. In addressing functionally relevant dynamics, the headgroups of phospholipids and their interac-

<sup>†</sup> This work was supported by the Medical Research Council Program grant G000852 to A.W.

\* To whom correspondence should be addressed. Tel: 44-1-865-275-268. Fax: 44-1-865-275-234. E-mail: anthony.watts@bioch.ox.ac.uk.

<sup>‡</sup> Current address: School of Food and Nutritional Sciences, University of Shizuoka, Yada 52-1, Shizuoka 422-8526, Japan.

<sup>1</sup> Abbreviations: bR, bacteriorhodopsin; PM, purple membrane; rh, relative humidity; CP, cross polarization; DD, dipolar decoupling; MAS, magic angle spinning; MAOSS, magic angle oriented sample spinning; PGP-Me, methyl phosphatidylglycerophosphate; PISEMA, polarization inversion spin exchange at the magic angle; HETCOR, heteronuclear correlation spectroscopy; IENS, incoherent elastic neutron scattering; S-TGA-1, triglycosyl lipid;  $T_1^P$ , the phosphorus spin–lattice relaxation times in the laboratory frame;  $T_2$ , spin–spin relaxation time;  $T_{1\rho}^H$ , the proton spin–lattice relaxation times in the rotating frame; PG, phosphatidylglycerol; PGS, phosphatidylglycerosulphate; BPG, archaeal cardiolipin; GlyC, archaeal glycocardioliipin; CSA, chemical shift anisotropy.

tion with a membrane receptor have not been well characterized, although protein–lipid interactions in the acyl chain region are generally considered to be important for the activity of membrane proteins and for maintaining the 3D structure (33–37). Detailed information on the dynamic properties of a membrane protein, accompanied or induced by conformational transitions during functional activity, and the involvement of membrane lipids is therefore required for a thorough understanding of the mechanisms and the rate-limiting steps of any functional process, namely, proton pumping for bR.

At ambient temperature, the correlation times of the local anisotropic motions of bR in the PM pellet are estimated to be  $10^{-4}$  s for the loops,  $10^{-2}$  s for the transmembrane  $\alpha$ -helices, and  $10^{-8}$  s for the C-terminus region protruding from the membrane surface, as determined by solid-state magic angle spinning (MAS) NMR (38). MAS NMR methods are thus very informative (in favorable cases in which assignment is achieved) in providing detailed local information about the dynamic range around selective regions within a membrane receptor. However, a problem arises because the resolved signals of individual residues in the MAS NMR spectra are broadened to show featureless signals at around 213 K (30), and thus local and specific information below this temperature is lost.

Incoherent elastic neutron scattering (IENS) methods revealed a dynamical transition at around 150 K and a hydration-dependent transition at 230 K, which correlates with nano- to pico-second motion to a softer, anharmonic atomic fluctuation regime in the global behavior of proteins (39–42). A comparison of the dynamics determined for different structural motifs or locations in bR may show some differences in the dynamics of cytoplasmically and extracellularly located segments of the transmembrane  $\alpha$ -helices in a quantitative way, as indicated qualitatively by electron (43) and X-ray (44) diffraction of bR in crystals and neutron scattering from PMs (39).

It has been shown from IENS studies that the local dynamics of bR is directly related to the hydration level of the membrane (39). Also, both the bR photocycle and proton pumping activity are accompanied by conformational changes in bR and are largely influenced by the extent of hydration (45, 46). Hydration in the plane of the membrane is considered to be predominantly around the lipid headgroups and in the proton channel (47, 48). In this study,  $^{15}\text{N}$ - and  $^{31}\text{P}$ -oriented NMR spectroscopy is used to determine the synergy between the dynamics of bR and the phospholipids in the PM from ambient temperature to 130 K with a variety of hydration levels. Because the spectra of  $^{15}\text{N}$ -amide labeled bR give separated signals from loops and transmembrane  $\alpha$ -helices in all temperature ranges (31, 32), it has been possible to compare the motional behavior of the transmembrane  $\alpha$ -helices and loops. By comparing  $^{15}\text{N}$  NMR spin–spin relaxation times ( $T_2$ ) of labeled residues, such molecular motions of around 10s  $\mu\text{s}$  in various regions of the protein could be determined. The oriented  $^{31}\text{P}$  static NMR spectra of PMs have also been used as indicators to characterize the mosaic spread of the oriented PM sample (24) to give information about the dynamic anisotropy of the headgroups of the major phospholipid (PGP-Me) in PMs. Importantly, the molecular motion around NMR-accessible time scales could be compared with known biological activity. Such

knowledge of molecular dynamics is vital for a mechanistic understanding of protein activity and is often not addressed in purely structural models based on measured conformational changes and reorientations in helical membrane proteins embedded in the natural lipid bilayer (49). The results, by correlating the dynamics and structural information on hydration, have permitted the exploration of the effect of water and temperature on protein dynamics in the functionally important range, and a connection with functionally significant dynamics has been made.

## MATERIALS AND METHODS

**Sample Preparation.** Natural abundance PM and [ $^{15}\text{N}$ ]Glycyl- or [ $^{15}\text{N}$ ]Met-labeled PM were obtained by growing *H. salinarium* strain S9 on a standard medium using pepton (L37, Oxoid, U.K.) (50) or a synthetic medium (51) containing L-[ $^{15}\text{N}$ ]Glycine or L-[ $^{15}\text{N}$ ]Methionine ( $^{15}\text{N}$ , 98%, Cambridge Isotope Laboratories, Andover, MA). After isolation and purification (50), the PM was suspended in either deionized water (pH of the solution is around 3; sample I), 5 mM sodium citrate buffer, KCl (pH 6.0; sample II), 5 mM HEPES–HCl buffer, NaCl (pH 7.0; sample III), or 10 mM HEPES–HCl buffer, NaCl (pH 7.0; sample IV), with a bR concentration of 3–4 mg/mL (11–15  $\mu\text{M}$ ). For the measurement of full width of  $^{31}\text{P}$  chemical shift anisotropy, suspension (II) was packed in a zirconia NMR rotor. Oriented PM films were prepared on thin glass plates (8  $\times$  8  $\times$  0.06–0.08 mm, Paul Marienfeld GmbH & Co. KG, Lauda-Königshofen, Germany) by slow evaporation of the suspensions in air. A total of  $\sim 10$  mg of bR was distributed over the surface of 10 to 12 plates. This film, made under exposure to ambient air, is referred to here as a dry sample. Otherwise, the PM films were placed in a desiccator at 310 K for 24 h to control the relative humidity (rh) of the PM films with saturated NaCl solutions (75% rh) or water (100% rh) (52). Saturated KCl solution was used to control the rh to 85% at 293 K (52) for five days. PM films formed on the thin glass plates or some other supports have been used for the structural and functional determination of bR by several spectroscopic and diffraction methods without recourse to further crystallization (47, 48, 53, 54). The lipid bilayers stack uniaxially parallel to the plates together with intercalating water layers to preserve the directional quality of the protein and to maintain the structural and functional integrity under a wide range of conditions, such as pH, temperature, humidity, and chemical environment (55). The hydrated PM films were stacked together and placed in the desiccator for another 24 h to ensure equilibrium. The stacked plates were sealed with parafilm and placed in polyethylene tubes (RS Components Ltd., Northants, U. K.) to maintain hydration during NMR measurements. The hydration level was maintained during the accumulation of NMR measurements as judged from the  $^{31}\text{P}$  NMR signals that are very sensitive to hydration levels (see below). For fully hydrated samples, a wet cotton wool ball was sealed together with the PM samples for long-term accumulation.

**NMR Measurement.** Phosphorus-31 and  $^{15}\text{N}$  static NMR spectra were measured on a Varian CMX Infinity 400 spectrometer with the resonance frequencies of 397.9, 161.1, and 40.3 MHz for  $^1\text{H}$ ,  $^{31}\text{P}$ , and  $^{15}\text{N}$  nuclei, respectively. For the solid-state NMR measurements on oriented membranes, glass plates were inserted into a home-built coil that is settled

perpendicular to the magnetic field ( $B_0$ ) and used to determine the conformation and orientation relative to the  $B_0$  of specifically labeled molecular segments. Pulse lengths of  $90^\circ$  and  $180^\circ$  for  $^1\text{H}$ ,  $^{31}\text{P}$ , and  $^{15}\text{N}$  were typically 5.0 and 10.0  $\mu\text{s}$ . For  $^{15}\text{N}$  and  $^{31}\text{P}$  cross polarization (CP) measurements, 1.0 ms contact time was used during CP with 50 kHz of spin-locking power, and 40–45 kHz continuous wave (CW) decoupling was calibrated at each temperature applied on the H channel.  $^{31}\text{P}$  static NMR measurements were acquired under Hahn-echo conditions, with a pulse sequence of  $90^\circ$ - $\tau$ - $180^\circ$ - $\tau_1$ -acquisition with proton decoupling. An echo interval ( $\tau$ ) of 20  $\mu\text{s}$  was used. Occasionally, for the dry sample and at low temperatures,  $^{31}\text{P}$  NMR spectra were also obtained using a pulse with a decoupling pulse sequence and CP.

The  $^{31}\text{P}$  and  $^{15}\text{N}$  chemical shifts were referenced at 0 ppm from external  $\text{H}_3\text{PO}_4$  and at 17.3 ppm from external  $\text{NH}_4\text{Cl}$  and saturated  $\text{NH}_4^+\text{NO}_3^-$  (56) solutions, respectively. Low-temperature experiments were performed using cooled nitrogen gas with ample time to achieve equilibrium of the sample. The actual sample temperature in the coil was calibrated using static  $^{207}\text{Pb}$  spectra of solid lead nitrate at various temperatures (57, 58) and turned out to be 91.4% compared to those indicated on the control device. All NMR measurements used 4 or 5 s recycle delays, and the number of acquisitions was between 3 and 9k scans for  $^{31}\text{P}$  and 1–20k scans for  $^{15}\text{N}$  NMR measurements unless noted otherwise. Lorentzian line broadening of 200 Hz was applied before Fourier transformation and carried out on 2k points after zero-filling.

The relaxation times measured by solid-state NMR spectroscopy ( $T_1$ ,  $T_2$ , and  $T_{1\rho}^{\text{H}}$ ) are useful in estimating the frequency of the molecular motion in the vicinity of the observed atoms or in the whole molecule. The phosphorus spin–lattice relaxation times in the laboratory frame ( $T_{1\rho}^{\text{P}}$ ) are sensitive to the motion with the frequency of the magnetic field strength ( $\sim 400$  MHz,  $\gamma_c \sim 2.5 \times 10^{-9}$  s) and give a measure of the dynamics of the phospholipids constituting the PM. The  $T_{1\rho}^{\text{P}}$  value was measured by the inversion–recovery method using a 0.001–6.0 s pulse duration at 293 K. For the dry sample,  $T_{1\rho}^{\text{P}}$  was measured by the method of CP enhancement with the inversion of spin temperature (59). The  $T_{1\rho}^{\text{P}}$  values were evaluated by a nonlinear least-squares fitting of the five data points of the  $^{31}\text{P}$  NMR signal intensities.

The proton spin–lattice relaxation times in the rotating frame ( $T_{1\rho}^{\text{H}}$ ) and the spin–spin relaxation times ( $T_2$ ) are directly related to proton local frequency ( $\sim 50$  kHz,  $\gamma_c \sim 2 \times 10^{-5}$  s), which may be close to the backbone motions of bR at physiological temperature. The  $T_{1\rho}^{\text{H}}$  values were evaluated by a nonlinear least-squares fitting of the  $^{15}\text{N}$  NMR signal intensities  $I(t)$  with 5–7 contact times with  $t$  between 0.1 and 8 ms according to eq 1, where  $I(0)$  denotes the initial peak intensities (60).

$$I(t) = \left[ \frac{I(0)}{T_{\text{N-H}}} \right] \frac{[\exp(-t/T_{1\rho}^{\text{H}}) - \exp(-t/T_{\text{N-H}})]}{[1/T_{\text{N-H}} - 1/T_{1\rho}^{\text{H}}]} \quad (1)$$

$^{15}\text{N}$  spin–spin relaxation times ( $T_2$ ) were measured by the Hahn-echo method together with CP and proton decoupling. The echo delay time was varied between 100 and 5000  $\mu\text{s}$ , and  $T_2$  was evaluated by a nonlinear least-squares fitting.

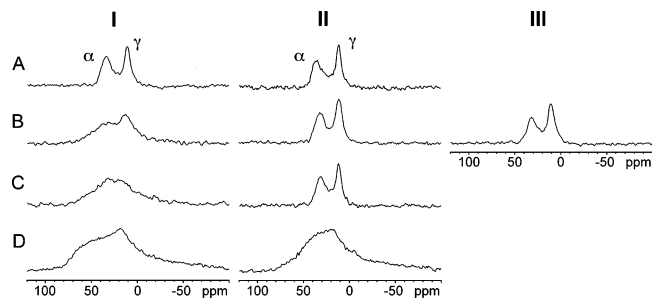


FIGURE 1:  $^{31}\text{P}$  chemical-shift echo spectra with proton decoupling for sample **I** (obtained from a water suspension), sample **II** (from a pH 6 suspension), and sample **III** (from a pH 7 suspension) with 100% (A), 85% (B), 75% relative humidity (rh) (C), and dry (D), respectively. The spectra were measured at 293 K.

## RESULTS

**$^{31}\text{P}$  NMR Studies.** Phosphorus-31 NMR spectroscopy has been used to determine the morphology of the phospholipids (37) and to identify the lipid content in reconstituted bR complexes (61). In PMs, the major phospholipid is methyl phosphatidylglycerophosphate (PGP-Me) (62), whose molar ratio to retinal was recently determined to be 2.4:1 (62).

Figure 1 shows the  $^{31}\text{P}$  static NMR spectra of PM films from water, pH 6 and pH 7 suspensions (**I–III**) with different rh measured at 293 K. In the spectra of samples **I–II** at 100% rh (Figure 1A), two signals around 40 and 13 ppm were observed, which can be assigned to the two phosphate groups of PGP-Me in PM,  $\alpha$ -phosphate (phosphodiester) and  $\gamma$ -phosphate (phosphomonoester) groups, respectively (24, 61). In the case of sample **I**, the  $^{31}\text{P}$  line shape changed predominantly, depending on the hydration level, and at 75% rh the signals were too broad and hardly separated into the two signals (Figure 1C). In contrast, little change of the line shapes was observed for sample **II** between 100 and 75% rh (Figures 1 and 2A). For all cases, the line widths of the  $\gamma$ -phosphate signals were less than those of the  $\alpha$ -phosphate signals because of the expected higher mobility of the  $\gamma$ -phosphates compared to that of the  $\alpha$ -groups (Figure 2A). The  $^{31}\text{P}$  NMR spectra from samples **III** and **IV** were very similar (data not shown), indicating the salt concentration of  $>1$  M may be high enough to neutralize the charges on the phosphate groups in the PM. However, the  $^{31}\text{P}$  static NMR spectra of dry films **I** and **II** showed broad signals (Figure 1D), not only from 50 to 0 ppm but also from 0 to  $-50$  ppm. When these samples were simply rehydrated, the signals recovered to the same spectral shape and width as those shown in Figure 1A–C.

Other phospholipids (phosphatidylglycerol (PG), phosphatidylglycerosulfate (PGS), archaeal cardiolipin (BPG), and archaeal glycardiolipin (GlyC)) containing  $\alpha$ -phosphate groups are present in PMs and gave ratios of the deconvoluted signal areas of the  $\alpha$ - (phosphodiester) and  $\gamma$ -phosphate (phosphomonoester) groups of 1.0:1 and 1.5:1 in samples **I** and **II** (100% rh), respectively.

The resonant line in the  $^{31}\text{P}$  NMR spectra from the  $\alpha$ - and  $\gamma$ -phosphate signals in samples **I** and **II** shifted gradually with increasing hydration levels (Figure 2B). The chemical shift anisotropy (CSA) tensor is axially symmetric for phospholipids undergoing fast rotation around an axis perpendicular to the bilayer plane. Here, using fully hydrated, random (unoriented) dispersions of PMs (pH 6), the full

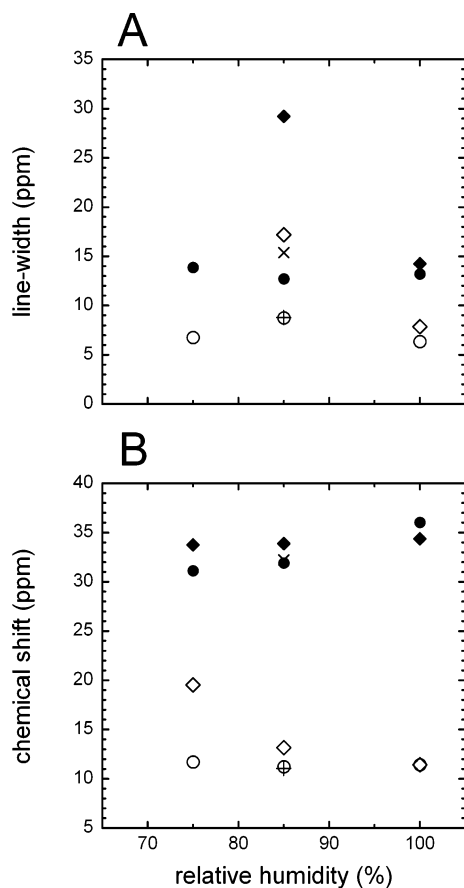


FIGURE 2: Line width of the <sup>31</sup>P NMR signals (A) and the chemical shifts (ppm) (B) observed in Figure 1 against relative humidity (rh). The α-phosphate signal of sample I (●); the γ-phosphate signal of sample I (◇); the α-phosphate signal of sample II (●); the γ-phosphate signal of sample II (○); the α-phosphate signal of sample III (×); and the γ-phosphate signal of sample III (+).

spectral width ( $\Delta\delta$ ) for the phosphodiester signal was determined to be 56 ppm (data not shown) at 293 K, which is in good agreement with previously determined data on PMs in a water suspension (24, 63). For a specific phospholipid in an oriented bilayer, the <sup>31</sup>P NMR spectrum consists of a single resonance line whose frequency  $\nu_{CSA}$  increased with the angle  $\theta$  between the membrane normal and the magnetic field ( $B_0$ ) according to (64)

$$\nu_{CSA}(\theta) = (2/3 \Delta\delta)(3 \cos^2 \theta - 1) \quad (2)$$

Using the chemical shifts of α-phosphate groups  $\Delta\delta$  and eq 2, the angles between the membrane normal and  $B_0$  were estimated to be 19.4, 18.1, and 8.7° at 75, 85, and 100% rh, respectively. In the case of the α-signal of I and the γ-signal of II, the chemical shifts did not change significantly (Figure 2B).

Table 1 summarizes the  $T_1^P$  values measured for the α- and γ-phosphate signals of samples I and II with different rh's at 293 K. The  $T_1^P$  values increased gradually as the hydration level decreased from 100 to 75% rh. The values obtained from the α-phosphate signals were larger than those of the γ-phosphate signals except for those of sample I at 75% rh (Table 1). For dry sample II, values that were 10 times larger were obtained for both signals compared with those from hydrated films (Table 1). It is expected that decreasing hydration will cause the reduced motion of both

Table 1: Spin-lattice Relaxation Times ( $T_1^P$ ; s) of α- and γ-phosphate Signals of PGP-Me in the PM Film (293 K)

	I		II	
	α	γ	α	γ
100% rh <sup>89</sup>	0.17 (±0.01)	0.09 (±0.006)	1.43 (±0.09)	1.01 (±0.05)
85% rh			1.84 (±0.18)	1.13 (±0.06)
75% rh <sup>89</sup>	4.29 (±0.30)	4.65 (±0.24)	1.96 (±0.12)	1.41 (±0.03)
dry			16.7 (±0.14) <sup>a</sup>	

<sup>a</sup> Obtained by the method of cross polarization enhancement with the inversion of spin temperature (59).

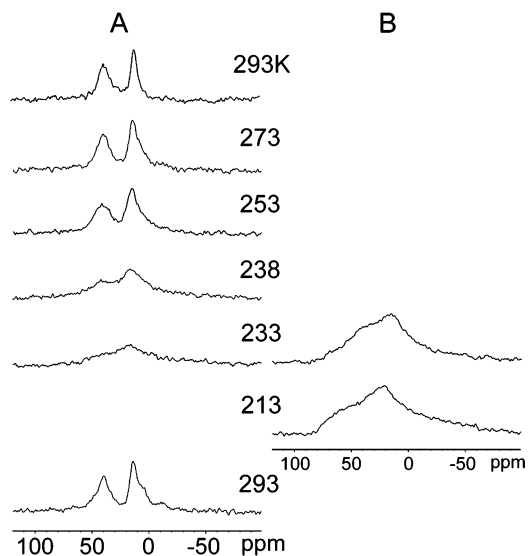


FIGURE 3: One pulse, decoupled <sup>31</sup>P NMR spectra (A) and CP spectra (B) of sample II at various temperatures between 293 and 213 K. The bottom spectrum (at 293 K) was measured after warming up the sample from 213 K.

headgroups, and in addition, the mobility of the γ-phosphate groups should be higher than that of the α-groups, with the frequency of the anisotropic motion at the long correlation side of the  $T_1$  minimum ( $\omega_0\tau_c \sim 1$ ;  $\tau_c \sim 2.5 \times 10^{-9}$  s). The  $T_1^P$  values for fully hydrated sample I were much smaller (faster) than those of II, although at 75% those measured for sample I were much longer (slower) than those of II.

**Temperature Variation of <sup>31</sup>P NMR Spectra.** As sample II (100% rh) was cooled, the line widths of the two <sup>31</sup>P signals increased gradually (Figure 3). When quantitated, the increase and decrease of the line widths from the spectra shown in Figure 3 and the signal intensities (Figure 4A and B, respectively) follow a two-step change: the first step is between 293 and 253 K and the second step is between 253 and 233 K, as shown by the dotted lines in Figure 4. Between 253 and 233 K, the signals became very broad, and the line shape became similar to that observed for the dry sample at 293 K (Figure 1D). The spectrum at 213 K had a broader resonance than that at 233 K, but the line shape did not change further and showed line widths closer to that of dry sample I at 293 K (Figure 1D). By warming up the samples slowly back to room temperature, the two signals from the two phosphates were reversibly recovered, although the line width of the γ-phosphate signal was slightly broader than that before cooling (Figure 3, bottom). Similar spectral changes occurred with sample I (data not shown).

**<sup>15</sup>N CP Spectra.** Figure 5 shows <sup>15</sup>N CP spectra of [<sup>15</sup>N]-Gly bR in the oriented PM from a PM suspension at pH 6

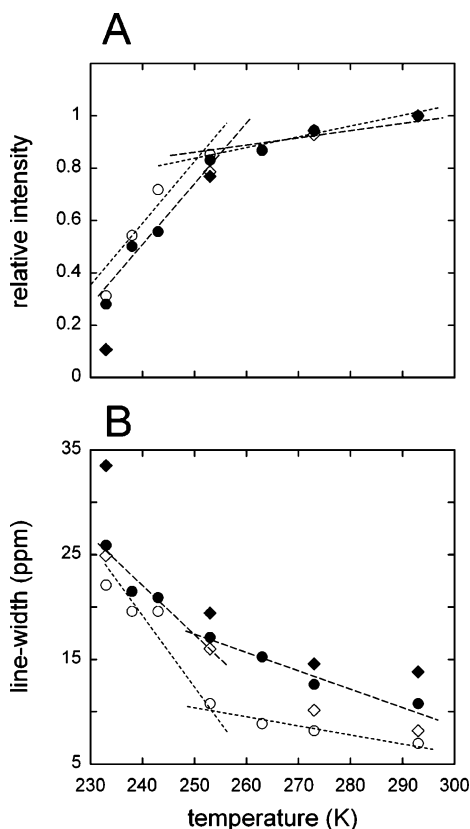


FIGURE 4: Plots of relative intensity normalized to the one obtained at 293 K as unity (A) and line width (B) of  $\alpha$ - and  $\gamma$ -phosphate groups at various temperatures. The plot style is the same as that in Figure 2. Changes for the solid and open circles are indicated by dotted lines.

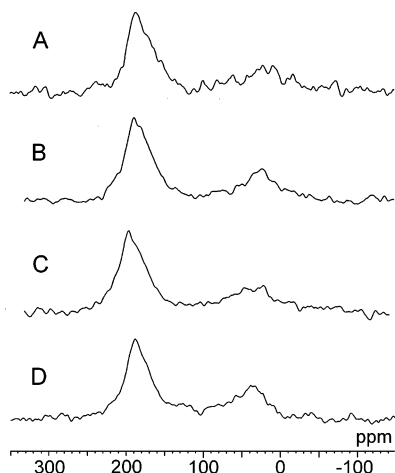


FIGURE 5:  $^{15}\text{N}$  CP spectra of  $[^{15}\text{N}]\text{Gly bR}$  from a pH 6 suspension (sample II) at 100% (A), 85% (B), and 75% rh (C) and dry samples (D). The spectra were measured at 293 K.

(II) measured at 293 K with different rh's. Although the  $^{31}\text{P}$  NMR spectra were sensitive to the hydration levels (Figure 1A–D) and were recorded using the  $^{15}\text{N}$  labeled protein in films at each hydration level, such large differences were not observed in the  $^{15}\text{N}$  NMR spectra. The signals from transmembrane  $\alpha$ -helices were observed around 150–220 ppm, which are close to the  $\delta_{\text{zz}}$  for an amide site (65, 66), and those from loops and the *N*- and *C*-termini regions are around 20–60 ppm. According to the 1C3W crystal structure of bR (8), there are 15 Gly residues in transmembrane  $\alpha$ -helices, 6 in the loops and a total of 5 in the *N*- and

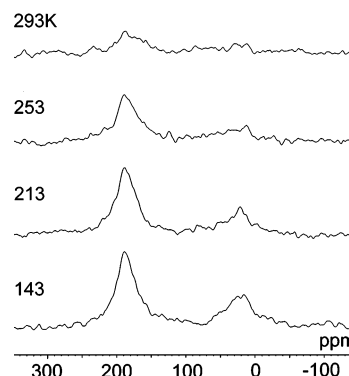


FIGURE 6:  $^{15}\text{N}$  CP spectra of  $[^{15}\text{N}]\text{Gly bR}$  from a pH 6 suspension at 100% rh at various temperatures. The spectra were accumulated with 4000 scans each.

Table 2: Proton Spin-Lattice Relaxation Times in the Rotating Frame ( $T_{1\rho}^{\text{H}}$ ; ms) of  $[^{15}\text{N}]\text{Gly bR}$  (from a pH 6 Suspension: Sample II)

	transmembrane $\alpha$ -helix <sup>a</sup>	loop <sup>b</sup>
rh100%		
293 K	4.48 $\pm$ 0.10 (182.4 ppm)	4.69 $\pm$ 0.49 (41.4 ppm) av 4.99 $\pm$ 1.28 (55.5 ppm)
253 K	6.54 $\pm$ 1.28 (185.2 ppm)	7.61 $\pm$ 0.35 (30.4 ppm) av 7.65 $\pm$ 0.59 (49.9 ppm)
213 K	6.52 $\pm$ 1.21 (184.8 ppm)	6.48 $\pm$ 2.78 (25.7 ppm) av 7.49 $\pm$ 2.89 (45.0 ppm)
173 K	11.3 $\pm$ 1.44 (187.8 ppm)	9.07 $\pm$ 1.16 (33.7 ppm) av 8.12 $\pm$ 1.10 (47.4 ppm)
133 K	13.6 $\pm$ 1.49 (185.8 ppm)	25.3 $\pm$ 15.1 (30.4 ppm) av 21.2 $\pm$ 17.0 (52.1 ppm)
rh75%		
293 K	8.38 $\pm$ 1.23 (189.1 ppm)	5.53 $\pm$ 1.09 (45.5 ppm) av 6.83 $\pm$ 3.64 (56.7 ppm)
dry		
293 K	5.75 $\pm$ 0.43 (187.8 ppm)	6.97 $\pm$ 0.19 (29.7 ppm) av 6.68 $\pm$ 0.97 (34.7 ppm)

<sup>a</sup> Obtained at the maximum resonance height from helices (the chemical shifts are in parentheses). <sup>b</sup> Obtained at the chemical shift shown in parenthesis for the resonances from the loops and/or the *N*- and *C*-termini together with the average of some other contributing resonances.

*C*-termini. However, the signals at 100% rh, especially from the loop signals, were small, and the signal areas did not match with the ratios from the numbers of residues. This signal reduction is probably due to the local mobility of the labeled residues in the range of the proton decoupling frequency (40–45 kHz) (67). The expected spectral ratio was recovered as the hydration levels were decreased. Also, the signals from the helices at 100% rh were rather spread out when compared with those from dry sample (Figure 5A and D). When the fully hydrated sample (II) was cooled, together with the increase of overall signal intensities, the signal areas from the loops (and termini) increased gradually (Figure 6). The line widths of the resonances from the  $\alpha$ -helices at 143 K (Figure 6) also decreased and looked similar to those observed for the dry sample at 293 K (Figure 5D).

$T_{1\rho}^{\text{H}}$  and  $T_2$  values are strongly associated with proton decoupling frequencies (45 kHz,  $\sim 20 \mu\text{s}$ ). The  $^{15}\text{N}$ -resolved  $T_{1\rho}^{\text{H}}$  values measured at several temperatures and at different rh's are summarized in Table 2. The  $T_{1\rho}^{\text{H}}$  values obtained were similar because of a rapid spin-diffusion process in the system except when anything existed to perturb the diffusion process. The values obtained for the helices are slightly smaller than those of the loops (and termini). The variation

Table 3:  $^{15}\text{N}$  Spin–Spin Relaxation Times ( $T_2$ ; ms) of [ $^{15}\text{N}$ ]Gly- or [ $^{15}\text{N}$ ]Met bR in the pH 6 Suspension for Sample II

	transmembrane $\alpha$ -helix	loop
$^{15}\text{N}$ ]Gly bR		
100% rh		
293 K	1.64 $\pm$ 0.12 (181.9 ppm)	0.90 $\pm$ 0.26 (48.9 ppm) av <sup>a</sup> 0.81 $\pm$ 0.24 (58.6 ppm)
273 K	1.66 $\pm$ 0.18 (174.7 ppm)	1.28 $\pm$ 0.34 (48.2 ppm) av 1.53 $\pm$ 0.32 (44.4 ppm)
243 K	3.44 $\pm$ 0.34 (175.8 ppm)	1.62 $\pm$ 0.18 (48.8 ppm) av 1.76 $\pm$ 0.17 (47.1 ppm)
213 K	3.09 $\pm$ 0.44 (180.9 ppm)	2.81 $\pm$ 0.50 (45.9 ppm) av 2.83 $\pm$ 0.51 (47.6 ppm)
173 K	4.09 $\pm$ 0.24 (181.9 ppm)	3.74 $\pm$ 0.55 (46.9 ppm) av 3.69 $\pm$ 0.81 (48.2 ppm)
133 K	5.58 $\pm$ 0.75 (185.9 ppm)	3.83 $\pm$ 0.74 (46.9 ppm) av 3.73 $\pm$ 0.74 (48.2 ppm)
75% rh		
293 K	2.26 $\pm$ 0.26 (181.9 ppm)	0.94 $\pm$ 0.14 (49.9 ppm) av 0.94 $\pm$ 0.14 (53.7 ppm)
dry		
293 K	4.49 $\pm$ 0.58 (175.4 ppm)	3.90 $\pm$ 1.47 (37.4 ppm) av 3.56 $\pm$ 1.12 (51.8 ppm)
$^{15}\text{N}$ ]Met bR		
100% rh		
293 K	1.87 $\pm$ 0.20 (186.7 ppm)	ND <sup>b</sup>
dry		
293 K	3.84 $\pm$ 0.47 (190.5 ppm)	2.98 $\pm$ 0.66 (44.4 ppm) av 2.75 $\pm$ 0.53 (47.0 ppm)

<sup>a</sup> Averaged out for the three to five data sets obtained at the indicated chemical shifts. <sup>b</sup> Signals were too small to analyze.

in the  $T_{1\rho}^{\text{H}}$  values may be within the orientational dependence of this relaxation time, reported to be 30% less at 90° than that at 0° (68). It is clear that the  $T_{1\rho}^{\text{H}}$  values became gradually longer as the sample was cooled, and because it can be expected that cooling reduces motional frequencies some motion(s) in bR in the time scale range of  $\sim 10^{-5}$  s for  $T_{1\rho}^{\text{H}}$  became slower and was gradually removed out of this time scale window. The values at 253 and 213 K for  $T_{1\rho}^{\text{H}}$  and those measured for the dry sample at 293 K were similar (Table 2). The  $^{15}\text{N}$   $T_2$  values under high-power proton decoupling were extremely short at 293 K (Table 3). As the sample was cooled, the  $T_2$  values from the  $\alpha$ -helical signals increased stepwise, from 273 to 243 and below 213 K, whereas those at 243 and 213 K were very similar (Table 3 and Figure 7). The significant changes in the  $T_2$  values of the loops might have occurred between 243 and 213 K. This data, especially at 243 and 213 K, was reproducible with different samples within the error range. It appears that decreasing the hydration levels, therefore, increases the  $^{15}\text{N}$   $T_2$  values (Table 3). However, the  $T_2$  values for the signals of the transmembrane regions of [ $^{15}\text{N}$ ]Met-bR in fully hydrated and dry conditions (Table 3) are very similar within the errors of measurement when compared with those obtained for [ $^{15}\text{N}$ ]Gly bR at 293 K.

## DISCUSSION

*Dynamics of Phospholipids in the PM.* Some of the native PM lipids in *H. salinarium* are carried with bR through its purification and even crystallization procedures by the use of detergents; therefore, it is suggested that those natural lipids are necessary to maintain the 2D PM lattice (69). Indeed bR-DMPC reconstitution, which contains only PGP-Me or PGS in the presence of  $>2$  M NaCl, showed the

crystalline array formation of the PM (70, 71), and reconstituted bR in model membranes without these natural lipids showed conformational changes induced by array formation (72). It seems, therefore, that a specific interaction of the protein with the charged phospholipids is important to maintain the 3D structure of PMs. Also, lipids sometimes play an important role in protein activity through lipid–protein interactions. Only fully lipidated membranes are known to display the flexibility in the pico to nanosecond time scale as shown in neuron studies (73). It has been suggested that PGP-Me is the major phospholipid in PMs and together with triglycosyl lipid (S-TGA-1) could be involved in the transport of protons across the extracellular surface of the PM to the red membrane for ensuing ATP synthesis (74, 75).

The linewidths of the  $^{31}\text{P}$  NMR signals (**I**: Figures 1 and 2A) clearly increased as hydration levels lowered. The PM films from a water/D<sub>2</sub>O suspension have been extensively studied by neutron scattering (76). It has been shown that the interbilayer spacing of the PM increases steeply from 49 Å for the completely dried films over P<sub>2</sub>O<sub>5</sub>, which corresponds to a membrane thickness of 52 Å at 75% rh (47, 48), to  $\sim 77$  Å at 100% rh (15, 48, 77). The hydration water is mainly associated with lipid headgroups at a high hydration level (78), and the removal of water around the lipid headgroups will cause a condensation of the lipid chains (47, 48). The  $^{31}\text{P}$  NMR results indicate that upon drying a loss of the interbilayer spacing could cause structural heterogeneity in the vicinity of the phosphate groups. However, the use of salts for the PM films (**II**) resulted in better alignment even at lower hydration levels (75% rh; Figure 1A–C). The pH of the samples was also different (**I**: pH  $\sim 3$ ; **II**: pH 6), causing a change in the surface charge of the PM at the lipid headgroups and the charged side chains of the protein (79). The effect of pH and salt on the PM surface has been examined using AFM (80), showing that upon drying the existence of salt, rather than changing pH, could stabilize the perturbations of surface morphology. It is suggested that the lipid headgroups may be shielded by the salt ions to permit better membrane alignment. This is also supported by the results of the  $T_{1\rho}^{\text{P}}$  values (Table 1), where the mobility of both  $\alpha$ - and  $\gamma$ -phosphate groups without salt (**I**) is higher than that with salt (**II**), when they are fully hydrated.

Upon cooling, the  $^{31}\text{P}$  NMR signals of the fully hydrated PM films became broader in two incremental steps between 293 and 253 K and between 253 and 233 K. It was reported that for a PM film made from a water suspension at low temperature ( $\sim 250$  K) the removal of excess water was seen to decrease the interbilayer spacing to  $\sim 53$  Å, which corresponds to bilayer thickness with one to two layers of (so-called nonfreezing) water (77). Also, freezing excess water has been observed at around 260 K (40). The first step of the change, between 293 and 253 K, observed in the  $^{31}\text{P}$  NMR spectra, may correspond to freezing of excess water (40). A significant broadening of the  $^{31}\text{P}$  NMR spectra at around 233 K (Figure 3) indicates a dynamic transition in the lipid headgroup motion. By neutron scattering, a dynamic transition at approximately 230 K between harmonic and nonharmonic motions was shown only for a hydrated PM sample (42). The spectral shape changes for the lipid headgroups observed (Figure 3) here may correspond to the

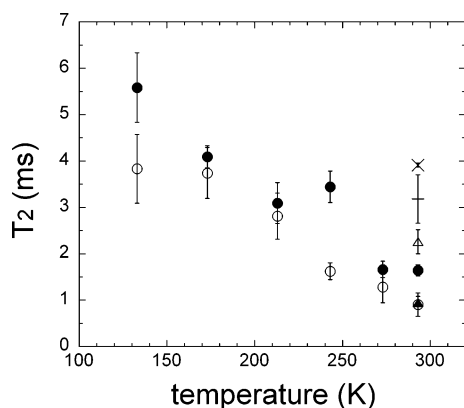


FIGURE 7: Plots of  $T_2$  values at a variety of temperatures (Table 3). Values obtained from the signals from transmembrane  $\alpha$ -helices (100% rh) (●); from the loops (100% rh) (○); from the signals from the helices (75% rh) (△); from loops (75% rh) (▲); from the signals from the helices (dry) (×); and from loops (dry) (+).

same dynamic transition. Because the  $^{31}\text{P}$  NMR spectrum at 233 K (Figure 3) is similar to that from the dry one (Figure 1D), and the line shape of the spectrum did not change below 233 K (Figure 3), the spectrum from the dry sample would not change any further on reduction of temperature. It is therefore suggested that the dynamic transition observed here would occur only for the hydrated sample. It should be emphasized that this transition between 253 and 233 K was seen for both samples with and without salt (Figures 3 and 4). It has been reported that dynamic changes of the fatty acid chains in the PM lipids also appeared at 233 and 163 K for the side and the terminal methyl groups of the lipids ((3*R*)-, (7*R*)-, and (11*R*)-15-tetramethylhexadecyl groups, respectively) but only in the presence of 10 mM NaCl (81).

**Dynamics of bR in the Oriented PM.** The protein dynamics of around 10s of  $\mu\text{s}$  was determined here at close to physiological conditions for the PM by controlling both salt and hydration. The relatively small  $T_{1\rho}^{\text{H}}$  values at 293 K in the fully hydrated PM suggest that there exists some group(s) with motions close to  $\sim 10^{-5}$  s, and from the  $T_2$  results, the fluctuation of the  $^{15}\text{NH}$  bonds could be the ones with this motional frequency of  $\sim 10^{-5}$  s. The result that not only the loops but also the helices have the motion close to  $\gamma_c \sim 10^{-5}$  s suggests that bR in the fully hydrated 2D crystals stacked on the glass plates may have motions that are different from those of PMs in suspension studied by MAS NMR (29, 82, 83).

Decreasing the hydration level gradually increased the  $T_2$  value obtained for the  $^{15}\text{N}$ -labeled transmembrane  $\alpha$ -helices (Table 3 and Figure 7). However, it is interesting to note that the  $T_2$  values for the loops at 100 and 75% rh were very similar, whereas those for the dry sample were larger than those at 100 and 75% rh (Table 3 and Figure 7). It has been reported that the conformational changes and proton pumping of bR is observed at 75% rh, although only one water layer is in direct contact with the membrane surface at this hydration level, and the photocycle is slowed (46, 84, 85). Also, at >75% rh, two new populations of water have been observed by  $^2\text{H}$  NMR, possibly correlating with the structural and functional transitions around this hydration level (86). In contrast, below 60% rh, the functional conformational changes in bR do not occur, and the photocycle cannot be completed (84). From the measurement here of  $T_2$  at 293 K,

it might be suggested that the mobility of loops with close to 10s  $\mu\text{s}$  is necessary to complete the photocycle of bR, even if the motion of transmembrane  $\alpha$ -helices is slightly restricted.

For the 100% rh sample, an increase in the  $T_2$  values for the  $^{15}\text{N}$ -labeled transmembrane  $\alpha$ -helices was observed between 273 and 243 and below 213 K (Table 3, Figure 7). This result suggests the freezing of excess water at around 260 K (40), which is associated with the reduction of interbilayer spacing (77), may cause a decrease in the mobility of the transmembrane helices. Dynamic changes of the loops might occur between 243 and 213 K, which could be the same temperature as that of the dynamic phase transition of the phosphate groups of PM lipids, as described above. The coupled transitions may suggest that interactions occur between the loops of bR and phospholipids, although protein–protein interactions between leaflets cannot be excluded because the stack could be  $\sim 53$  Å at 250 K at full hydration (77). Incoherent IENS for smaller scattering vectors in bR have revealed another dynamic transition around 150 K, which is present for both the dry and fully hydrated membranes (39–41). This transition was not observed in the  $T_2$  measurements here for  $^{15}\text{N}$ -labeled protein, suggesting that this may be due to the difference in the frequency range sensitivity of  $T_2$ .

The importance of temperature together with hydration on the proton pump activity of bR is well known. Recent results from fully  $^{15}\text{N}$ -labeled bR at 86% rh showed slightly longer  $T_2$  values at any temperature for the helix signals (87) than those from fully hydrated samples. Zaccai has suggested that the inhibition of bR activity at low temperatures or in the dry state could be due to a reduction of motions from the close packing of lipids around the protein in PMs (47). Not only the interbilayer spacing but also the in-plane unit cell parameter (defined as the length of the trimer unit of bR in the lattice) decreases about 1 Å for the completely dried film compared with that of a fully hydrated film (15, 47, 48, 77, 78). The decay of the M-intermediate in the photocycle and the regeneration of the ground state are strongly slowed below 80% rh (46). The decay of the multiple M-states can also be locked around 220–260 K (88). It is interesting to note that the  $T_2$  values at 243 and 213 K of the transmembrane  $\alpha$ -helices for the fully hydrated PM were longer than those at 293 and 273 K, and the  $T_2$  values of loops increased between 243 and 213 K (Table 3, Figure 7). Furthermore, at 100% rh, the  $T_2$  values of both transmembrane helices and loops obtained at 213 K were close to those obtained from the dry sample at 293 K (Figure 7) in which no proton pumping activity or conformational changes of the protein were observed (84). It could therefore be suggested that the loss of motional flexibility with 10s of  $\mu\text{s}$  for not only the transmembrane  $\alpha$ -helices but also the loops could stop the photocycle at the M-state where the biggest conformational changes should occur. Therefore, it can be concluded that the molecular motion of loops close to  $\sim 10^{-5}$  s is necessary to complete the bR photocycle, and if both loops and transmembrane  $\alpha$ -helices lose this flexibility, the cycle is trapped.

Methionine residues are located predominantly in the extracellular half of the bR except for Met-163, which is in a loop. It has been shown by an environmental force constant measured by neutron scattering (40, 41), Debye–Waller

factors from electron diffraction (43), and from X-ray diffraction of bR crystals (44) that the motional fluctuations within bR are smaller in the extracellular half of bR than in the cytoplasmic half, especially at room temperature. Although the Gly residues are located not only in the extracellular half but also in the cytoplasmic part of the transmembrane helices, at 293 K, the  $T_2$  relaxation times obtained from the Met-labeled sample were very similar (within the error range) to those obtained from the Gly-labeled sample (Table 2). It is suggested that for motions in the correlation time range of  $\sim 10^{-5}$  s, the mobility of the cytoplasmic half of bR is similar to that of the extracellular half.

The  $^{15}\text{N}$   $T_2$  values are also affected by the interference between random motion and coherent decoupling or by spinning frequencies. Therefore, some spectral components should be modulated by, for example, the transverse component due to static H–X dipolar interactions, and are due to the fluctuation of dipolar and/or chemical shift interactions (67, 89, 90). In the case of the oriented static  $^{15}\text{NH}$  signals, motional modulation of the chemical shift interaction could be eliminated, (although it is dominant for the case of carbonyl nuclei in  $^{13}\text{C}$  CP-MAS NMR measurements) and it should shorten  $T_2$  at low temperatures without MAS. For  $^{15}\text{N}$   $T_2$  values, the N–H dipolar interaction could dominate, as seen when  $T_2$  is gradually increased at low temperature (Figure 7). Therefore, at 293 K, proton decoupling was not effective because of an interference of the frequency of molecular motion with the frequency of the NH fluctuations (91), resulting in the poor signal-to noise ratio of  $^{15}\text{N}$  CP spectrum, which recovered gradually by cooling, as the molecular motion became slower (Figure 5). However, here, the dipole–dipole interactions are dependent on the dipolar orientation. The difference in  $^{15}\text{N}$   $T_2$  values between the signals from the transmembrane helices and loops may not be directly assigned to the difference in the protein mobility. Also,  $T_2$  is closely related to the line width of the NMR signals. Calculations using the  $T_2$  values indicate that the line width from the fully hydrated sample should be  $\sim 200$  Hz for the transmembrane  $\alpha$ -helices and  $\sim 400$  Hz for the loops, and even at 133 K, the resonance should be broad ( $\sim 85$  Hz). Such intrinsic mobility of membrane proteins in membranes has been shown to cause spectral interpretational difficulties in the 2D static NMR measurement (31, 49), and an intricate link between membrane dynamics and hydration has been demonstrated here for both proteins and lipids, as shown previously for lipids only in the bilayers (92).

## ACKNOWLEDGMENT

We acknowledge Dr. Xin Zhao (University of Oxford, U.K.), Dr. Boyan Bonev (University of Nottingham, U.K.), and Professor Akira Naito (Yokohama National University, Japan) for useful discussions.

## REFERENCES

- Ovchinnikov, Y. (1982) Rhodopsin and bacteriorhodopsin: structure-function relationships, *FEBS Lett.* 148, 179–191.
- Stoeckenius, W., and Bogomolni, R. A. (1982) Bacteriorhodopsin and related pigments of Halobacteria, *Annu. Rev. Biochem.* 1982, 587–616.
- Mathies, R. A., Lin, S. W., Ames, J. B., and Pollard, W. T. (1991) From femtoseconds to biology: mechanism of bacteriorhodopsin's light-driven proton pump, *Annu. Rev. Biophys. Biophys. Chem.* 20, 491–518.
- Lanyi, J. K. (1997) Mechanism of ion transport across membrane. Bacteriorhodopsin as a prototype for proton pump, *J. Biol. Chem.* 272, 31209–31212.
- Lanyi, J. K. (1993) Proton translocation mechanism and energetics in the light-driven pump bacteriorhodopsin, *Biochim. Biophys. Acta* 1460, 133–156.
- Essen, L., Siebert, R., Lehmann, W. D., and Oesterhelt, D. (1998) Lipid patches in membrane protein oligomers: crystal structure of the bacteriorhodopsin-lipid complex, *Proc. Natl. Acad. Sci. U.S.A.* 95, 11673–11678.
- Luecke, H., Richter, H. T., and Lanyi, J. K. (1998) Proton-transfer pathways in bacteriorhodopsin at 2.3 angstrom resolution, *Science* 280, 1934.
- Luecke, H., Schobert, B., Richter, H. T., Cartailler, J. P., and Lanyi, J. K. (1999) Structure of bacteriorhodopsin at 1.55 Å resolution, *J. Mol. Biol.* 291, 899–911.
- Sato, H., Takeda, K., Tani, K., Hino, T., Okada, T., Nakasako, M., Kamiya, N., and Kouyama, T. (1999) Specific lipid-protein interactions in a novel honeycomb lattice structure of bacteriorhodopsin, *Acta Crystallogr., Sect. D* 55, 1251–1256.
- Faham, S., and Bowie, J. U. (2002) Bicelle crystallization: a new method for crystallizing membrane proteins yields a monomeric bacteriorhodopsin structure, *J. Mol. Biol.* 316, 1–6.
- Schobert, B., Cupp-Vickery, J., Hornak, V., Smith, S., and Lanyi, J. (2002) Crystallographic structure of the K intermediate of bacteriorhodopsin: conservation of free energy after photoisomerization of the retinal, *J. Mol. Biol.* 321, 715–726.
- Mitsuoka, K., Hirai, T., Murata, K., Miyazawa, A., Kidera, A., Kimura, Y., and Fujiyoshi, Y. (1999) The structure of bacteriorhodopsin at 3.0 Å resolution based on electron crystallography: implication of the charge distribution, *J. Mol. Biol.* 286, 861–882.
- Subramaniam, S., and Henderson, R. (2000) Molecular mechanism of vectorial proton translocation by bacteriorhodopsin, *Nature* 406, 653–657.
- Dencher, N. A., Dresselhaus, D., Zaccari, G., and Buldt, G. (1989) Structural changes in bacteriorhodopsin during proton translocation revealed by neutron diffraction, *Proc. Natl. Acad. Sci. U.S.A.* 86, 7876–7879.
- Weik, M., Zaccari, G., Dencher, N. A., Oesterhelt, D., and Hauss, T. (1998) Structure and hydration of the M-state of the bacteriorhodopsin mutant D96N studied by neutron diffraction, *J. Mol. Biol.* 275, 625–634.
- Edman, K., Nollert, P., Royant, A., Belrhali, H., Pebay-Peyroula, E., Hajdu, J., Neutze, R., and Landau, E. M. (1999) High-resolution X-ray structure of an early intermediate in the bacteriorhodopsin photocycle, *Nature* 401, 822–826.
- Luecke, H., Schobert, B., Cartailler, J. P., Richter, H. T., Rosengarth, A., Needleman, R., and Lanyi, J. K. (2000) Coupling photoisomerization of retinal to directional transport in bacteriorhodopsin, *J. Mol. Biol.* 300, 1237–1255.
- Sass, H., Buldt, G., Gessenich, R., Hehn, D., Neff, D., Schlesinger, J., Berendzen, J., and Ormos, P. (2000) Structural alterations for proton translocation in the M state of wild-type bacteriorhodopsin, *Nature* 40, 649–653.
- Facciotti, M. T., Rouhani, S., Burkard, F. T., Betancourt, F. M., Downing, K. H., Rose, R. B., McDermott, G., and Glaeser, R. M. (2001) Structure of an early intermediate in the M-state phase of the bacteriorhodopsin photocycle, *Biophys. J.* 81, 3442–3455.
- Royant, A., Edman, K., Ursby, T., Pebay-Peyroula, E., Landau, E. M., and Neutze, R. (2001) Spectroscopic characterization of bacteriorhodopsin's L-intermediate in 3D crystals cooled to 170 K, *Photochem. Photobiol.* 74, 794–804.
- Lanyi, J., and Schobert, B. (2002) Crystallographic structure of the retinal and the protein after deprotonation of the Schiff base: the switch in the bacteriorhodopsin photocycle, *J. Mol. Biol.* 321, 727–737.
- Lanyi, J. K. (2004) Bacteriorhodopsin, *Annu. Rev. Physiol.* 66, 11.1–11.24.
- Lanyi, J. K., and Schobert, B. (2003) Mechanism of proton transport in bacteriorhodopsin from crystallographic structures of the k, L, m(1), m(2), and m(2)' intermediates of the photocycle, *J. Mol. Biol.* 328, 439–450.
- Ulrich, A. S., Heyn, M. P., and Watts, A. (1992) Structure determination of the cyclohexene ring of retinal in bacteriorhodopsin by solid-state deuterium NMR, *Biochemistry* 31, 10390–10399.

25. Ulrich, A. S., Wallat, I., Heyn, M. P., and Watts, A. (1995) Reorientation of retinal in the M-photointermediate of bacteriorhodopsin, *Nat. Struct. Biol.* 2, 190–192.
26. Herzfeld, J., and Tounge, B. (2000) NMR probes of vectoriality in the proton-motive photocycle of bacteriorhodopsin: evidence for an 'electrostatic steering' mechanism, *Biochim. Biophys. Acta* 1460, 95–105.
27. Herzfeld, J., and Lansing, J. C. (2002) Magnetic resonance studies of the bacteriorhodopsin pump cycle, *Annu. Rev. Biophys. Biomol. Struct.* 31, 73–95.
28. Saito, H., Tuzi, S., Yamaguchi, S., Tanio, M., and Naito, A. (2000) Conformation and backbone dynamics of bacteriorhodopsin revealed by <sup>13</sup>C-NMR, *Biochim. Biophys. Acta* 1460, 39–48.
29. Saito, H., Tuzi, S., Tanio, M., and Naito, A. (2002) Dynamic aspect of membrane proteins and membrane associated peptides as revealed by <sup>13</sup>C NMR: lessons from bacteriorhodopsin as an intact protein, *Annu. Rep. NMR Spectrosc.* 47, 39–108.
30. Saito, H., Tuzi, S., and Naito, A. (1998) Empirical vs. nonempirical evaluation of secondary structure of fibrous and membrane proteins *Annu. Rep. NMR Spectrosc.* 36, 79–121.
31. Kamihira, M., Vosegaard, T., Mason, A. J., Straus, S., Nielsen, N. C., and Watts, A. (2005) Structural and orientational constraints on bacteriorhodopsin in purple membranes determined by oriented-sample solid-state NMR spectroscopy, *J. Struct. Biol.* 149, 7–16.
32. Mason, A. J., Grage, S. L., Straus, S. K., Glaubitz, C., and Watts, A. (2004) Identifying anisotropic constraints in multiply labelled bacteriorhodopsin by <sup>15</sup>N MAOSS NMR: A general approach to structural studies of membrane proteins, *Biophys. J.* 86, 1610–1617.
33. Watts, A., and de Pont, J. J. H. H. M. (1985), *Protein-Lipid Interactions I*, Elsevier, Amsterdam.
34. Watts, A., and de Pont, J. J. H. H. M. (1986), *Protein-Lipid Interactions II*, Elsevier, Amsterdam.
35. Watts, A., and Van Gorkom, L. C. M. (1991) Surface organization of lipid bilayers, in *The Structure of Biological Membranes* (Yeagle, P., Ed.) pp 307–377, CRC Press, Boca Raton, FL.
36. Watts, A. (1993) Magnetic resonance studies of phospholipid-protein interactions in bilayers, in *Phospholipids Handbook* (Cevc, G., Ed.) pp 687–740, Marcel Dekker, New York.
37. Watts, A. (1998) Solid-state NMR approaches for studying the interaction of peptides and proteins with membranes, *Biochim. Biophys. Acta* 1376, 297–318.
38. Yamaguchi, S., Yonebayashi, K., Konishi, H., Tuzi, S., Naito, A., Lanyi, J. K., Needleman, R., and Saito, H. (2001) Cytoplasmic surface structure of bacteriorhodopsin consisting of interhelical loops and C-terminal alpha helix, modified by a variety of environmental factors as studied by (<sup>13</sup>)C-NMR, *Eur. J. Biochem.* 268, 2218–2228.
39. Lehnert, U., Reat, V., Weik, M., Zaccai, G., and Pfister, C. (1998) Thermal motions in bacteriorhodopsin at different hydration levels studied by neutron scattering: correlation with kinetics and light-induced conformational changes, *Biophys. J.* 75, 1945–1952.
40. Reat, V., Patzelt, H., Ferrand, M., Pfister, C., Oesterheld, D., and Zaccai, G. (1998) Dynamics of different functional parts of bacteriorhodopsin: H-2H labeling and neutron scattering, *Proc. Natl. Acad. Sci. U.S.A.* 95, 4970–4975.
41. Zaccai, G. (2000) How soft is a protein? A protein dynamics force constant measured by neutron scattering, *Science* 288, 1604–1607.
42. Ferrand, M., Dianouz, A. J., Petry, W., and Zaccai, G. (1993) Thermal motions and function of bacteriorhodopsin in purple membranes; effects of temperature and hydration studied by neutron scattering, *Proc. Natl. Acad. Sci. U.S.A.* 90, 9668–9672.
43. Grigorieff, N., Beckmann, E., and Zemlin, F. (1995) Lipid location in deoxycholate-treated purple membrane at 2.6 Å, *J. Mol. Biol.* 254, 404–415.
44. Belrhali, H., Nollert, P., Royant, A., Menzel, C., Rosenbusch, J. P., Landau, E. M., and Pebay-Peyroula, E. (1999) Protein, lipid and water organization in bacteriorhodopsin crystals: a molecular view of the purple membrane at 1.9 Å resolution, *Structure Fold Des.* 7, 909–917.
45. Korenstein, R., and Hess, B. (1977) Hydration effects on the photocycle of bacteriorhodopsin in thin layers of purple membrane, *Nature* 270, 184–186.
46. Sass, H. J., Schachowa, I. W., Rapp, G., Koch, M. H., Oesterheld, D., Dencher, N. A., and Buldt, G. (1997) The tertiary structural changes in bacteriorhodopsin occur between M states: X-ray diffraction and Fourier transform infrared spectroscopy, *EMBO J.* 16, 1484–1491.
47. Zaccai, G. (1987) Structure and hydration of purple membranes in different conditions, *J. Mol. Biol.* 194, 569–572.
48. Papadopoulos, G., Dencher, N. A., Zaccai, G., and Buldt, G. (1990) Water molecules and exchangeable hydrogen ions at the active centre of bacteriorhodopsin localized by neutron diffraction. Elements of the proton pathway? *J. Mol. Biol.* 214, 15–19.
49. Straus, S. K., Scott, W. R. P., and Watts, A. (2003) Assessing the effects of time and spatial averaging in <sup>15</sup>N chemical shift/<sup>15</sup>N-<sup>1</sup>H dipolar correlation solid-state NMR experiments, *J. Biomol. NMR* 26, 283–295.
50. Oesterheld, D., and Stoekenius, W. (1974) Isolation of the cell membrane of *Halobacterium halobium* and its fractionation into red and purple membrane, *Methods Enzymol.* 31, 667–678.
51. Helgerson, S. L., Siemsen, S. L., and Dratz, E. A. (1992) Enrichment of bacteriorhodopsin with isotopically labeled amino acids by biosynthetic incorporation in *Halobacterium halobium*, *Can. J. Microbiol.* 38, 1181–1185.
52. O'Brien, F. E. M. (1948) The control of humidity by saturated salt solutions, *J. Sci. Instrum.* 25, 73–76.
53. Seiff, F., Wallat, I., Ermann, P., and Heyn, M. P. (1985) A neutron diffraction study on the location of the polyene chain of retinal in bacteriorhodopsin, *Proc. Natl. Acad. Sci. U.S.A.* 82, 3227–3231.
54. Fitter, J., Lechner, R. E., and Dencher, N. A. (1999) Interactions of hydration water and biological membranes studied by neutron scattering, *J. Phys. Chem. B* 103, 8036–8050.
55. Oesterheld, D., Brauchle, C., and Hampp, N. (1991) Bacteriorhodopsin: a biological material for information processing, *Q. Rev. Biophys.* 24, 425–478.
56. Shoji, A., Ozaki, T., Fujito, T., Deguchi, K., Ando, S., and Ando, I. (1990) <sup>15</sup>N chemical shift tensors and conformation of solid polypeptides containing <sup>15</sup>N-labeled L-alanine residues by <sup>15</sup>N NMR. 2. secondary structure reflected in sigma22, *J. Am. Chem. Soc.* 112, 4693–4697.
57. Bielecki, A., and Burum, D. (1995) Temperature dependence of <sup>207</sup>Pb MAS spectra of solid lead nitrate. An accurate, sensitive thermometer for variable-temperature MAS, *J. Magn. Res. A* 116, 215–220.
58. Beckmann, P. A., and Dybowski, C. (2000) A thermometer for nonspinning solid-state NMR spectroscopy, *J. Magn. Res.* 146, 379–380.
59. Torchia, D. A. (1978) The measurement of proton-enhanced carbon-13 T1 values by a method which suppresses artifacts, *J. Magn. Res.* 30, 613–616.
60. Mehring, M. (1983) *High-Resolution Solid State NMR Spectroscopy in Solids*, Springer-Verlag, New York.
61. Gale, P., and Watts, A. (1991) Characterization of phospholipid compositions and physical properties of DMPC/bacteriorhodopsin vesicles produced by a detergent-free method, *Biochem. Biophys. Res. Commun.* 180, 939–944.
62. Kates, M., Kushwaha, S. C., and Sprott, G. D. (1982) Lipids of purple membrane from extreme halophiles and of methanogenic bacteria, *Methods Enzymol.* 88, 98–111.
63. Ekiel, I., Marsh, D., Smallbone, B. W., Kates, M., and Smith, I. C. (1981) The state of the lipids in the purple membrane of *Halobacterium cutirubrum* as seen by <sup>31</sup>P NMR, *Biochem. Biophys. Res. Commun.* 100, 105–110.
64. Seelig, J. (1978) <sup>31</sup>P nuclear magnetic resonance and the head-group structure of phospholipids in membranes, *Biochim. Biophys. Acta* 515, 105–140.
65. Teng, G., and Cross, T. A. (1989) Tensor orientation in a polypeptide, *J. Magn. Res.* 85, 439–447.
66. Cross, T. A., and Opella, S. J. (1994) Solid-state NMR structural studies of peptides and proteins in membranes, *Curr. Opin. Struct. Biol.* 4, 574–581.
67. Rothwell, W. P., and Waugh, J. S. (1981) Transverse relaxation of dipolar coupled spin systems under rf irradiation: Detecting motions in solids, *J. Chem. Phys.* 74, 2721–2732.
68. Separovic, F., Cornell, B., and Pace, R. (2000) Orientation dependence of NMR relaxation time, T1r, in lipid bilayers, *Chem. Phys. Lipids* 107, 159–167.
69. Cartailier, J. P., and Luecke, H. (2003) X-ray crystallographic analysis of lipid-protein interactions in the bacteriorhodopsin purple membrane, *Annu. Rev. Biomol. Struct.* 32, 285–310.
70. Sternberg, B., L'Hostis, C., Whiteway, C. A., and Watts, A. (1992) The essential role of *Halobacterium halobium* lipids in 2D-array formation of bacteriorhodopsin, *Biochim. Biophys. Acta* 1108, 21–30.

71. Watts, A. (1995) Bacteriorhodopsin: the mechanism of 2D-array formation and the structure of retinal in the protein, *Biophys. Chem.* 55, 137–151.
72. Saito, H., Yamamoto, Y., Tuzi, S., and Yamaguchi, S. (2003) Backbone dynamics of membrane proteins in lipid bilayers: the effect of two-dimensional array formation as revealed by site-directed solid-state  $^{13}\text{C}$  NMR studies on  $[3-^{13}\text{C}]\text{Ala}$ - and  $[1-^{13}\text{C}]\text{Val}$ -labeled bacteriorhodopsin, *Biochim. Biophys. Acta* 1616, 127–136.
73. Fitter, J., Ernst, O. P., Hauss, T., Lechner, R. E., Hofmann, K. P., and Dencher, N. A. (1998) Molecular motions and hydration of purple membranes and disk membranes studied by neutron scattering, *Eur. Biophys. J.* 27, 638–645.
74. Falk, K. E., Karlsson, K. A., and Samuelsson, B. E. (1980) Structural analysis by mass spectrometry and NMR spectroscopy of the glycolipid sulfate from *Halobacterium salinarium* and a note on its possible function, *Chem. Phys. Lipids* 27, 9–21.
75. Teissie, J., Prats, M., LeMassu, A., Stewart, L. C., and Kates, M. (1990) Lateral proton conduction in monolayers of phospholipids from extreme halophiles, *Biochemistry* 29, 59–65.
76. Gabel, F., Bicout, D., Lehnert, U., Tehei, M., Weik, M., and Zaccai, G. (2002) Protein dynamics studied by neutron scattering, *Q. Rev. Biophys.* 35, 327–367.
77. Lechner, R. E., Fitter, J., Dencher, N. A., and Hauss, T. (1998) Dehydration of biological membranes by cooling: an investigation on the purple membrane, *J. Mol. Biol.* 277, 593–603.
78. Fitter, J., Lechner, R. E., and Dencher, N. A. (1997) Influence of lipids on the dynamical behaviour of bacteriorhodopsin in the purple membrane., in *Biological Macromolecular Dynamics* (Cusack, S., Büttner, H., Ferrand, M., Lagan, M., and Timmins, P., Eds.) pp 123–128, Adedine Press, Schenectady, NY.
79. Gale, P., and Watts, A. (1992) Effect of bacteriorhodopsin on the orientation of the headgroup of 1,2-dimyristoyl-*sn*-glycero-3-phosphocholine in bilayers - a  $^{31}\text{P}$  and  $^2\text{H}$ -NMR study, *Biochim. Biophys. Acta* 1106, 317–324.
80. Voitchovsky, K., Contera, S. A., Kamihira, M., Watts, A., and Ryan, J. (2006) Differential stiffness and lipid mobility in the leaflets of purple membranes, *Biophys. J.* 90, 2075–2085.
81. Tuzi, S., Naito, A., and Saito, H. (1996) Temperature-dependent conformational change of bacteriorhodopsin as studied by solid-state  $^{13}\text{C}$  NMR, *Eur. J. Biochem.* 239, 294–301.
82. Tanio, M., Inoue, S., Yokota, K., Seki, T., Tuzi, S., Needleman, R., Lanyi, J., Naito, A., and Saito, H. (1999) Long-distance effects of site-directed mutations on backbone conformation in bacteriorhodopsin from solid-state NMR of  $[1-^{13}\text{C}]\text{Val}$ -labeled proteins, *Biophys. J.* 77, 431–442.
83. Tuzi, S., Naito, A., and Saito, H. (1994)  $^{13}\text{C}$  NMR study on conformation and dynamics of the transmembrane alpha-helices, loops, and C-terminus of  $[3-^{13}\text{C}]\text{Ala}$ -labeled bacteriorhodopsin, *Biochemistry* 33, 15046–15052.
84. Zaccai, G. (2004) The effects of water on protein dynamics, *Philos. Trans. Soc. London, Ser. B* 359, 1269–1275.
85. Varo, G., and Lanyi, J. K. (1991) Distortions in the photocycle of bacteriorhodopsin at moderate dehydration, *Biophys. J.* 59, 313–322.
86. Bechinger, B., and Weik, M. (2003) Deuterium solid-state NMR investigations of exchange labeled oriented purple membrane at different hydration levels, *Biophys. J.* 85, 361–369.
87. Soubias, O., Reat, V., Saurel, O., and Milon, A. (2004)  $^{15}\text{N}$  T2' relaxation times of bacteriorhodopsin transmembrane amide nitrogens, *Magn. Reson. Chem.* 42, 212–217.
88. Ormos, P. (1991) Infrared spectroscopic demonstration of a conformational change in bacteriorhodopsin involved in proton pumping, *Proc. Natl. Acad. Sci. U.S.A.* 88, 473–477.
89. Suwelack, D., Rothwell, W. P., and Waugh, J. S. (1980) Slow molecular motion detected in the NMR spectra of rotating solids, *J. Chem. Phys.* 74, 2559–2569.
90. Naito, A., Fukutani, A., Uitdehaag, M., Tuzi, S., and Saito, H. (1998) Backbone dynamics of polycrystalline peptides studied by measurements of  $^{15}\text{N}$  NMR lineshapes and  $^{13}\text{C}$  transverse relaxation times. *J. Mol. Struct.* 441, 231–241.
91. Saito, H., Yamaguchi, S., Okuda, H., Shiraiishi, A., and Tuzi, S. (2004) Dynamic aspect of bacteriorhodopsin as a typical membrane protein as revealed by site-directed solid-state  $^{13}\text{C}$  NMR, *Solid State Nucl. Magn. Reson.* 25, 5–14.
92. Ulrich, A. S., and Watts, A. (1994) Lipid headgroup hydration by  $^2\text{H}$ -NMR: a link between spectroscopy and thermodynamics, *Biophys. Chem.* 49, 39–50.

BI051756J